



Article

Bus Lane Design Based on Actual Traffic Loads and Climate Conditions

Giulia Del Serrone , Paola Di Mascio , Giuseppe Loprencipe , Lorenzo Vita and Laura Moretti *

Department of Civil, Constructional and Environmental Engineering, Sapienza University of Rome, Via Eudossiana 18, 00184 Rome, Italy; giulia.delserrone@uniroma1.it (G.D.S.); paola.dimascio@uniroma1.it (P.D.M.); giuseppe.loprencipe@uniroma1.it (G.L.); lorenzo.vita@uniroma1.it (L.V.)

* Correspondence: laura.moretti@uniroma1.it; Tel.: +39-06-44585114

Abstract: Bus lanes play a crucial role in urban areas as their primary objective is to increase public transport efficiency and help traffic and public transit systems flow more smoothly. This study starts with traffic and climate monitoring to verify asphalt bus lanes in Rome, Italy, according to the Italian Pavement Design Catalogue published in 1995. KENLAYER software calculated the stress-strain conditions under real traffic loads (i.e., hourly passages of urban buses, considering their axle load and seat occupancy rate), typical subgrade bearing capacity (i.e., resilient modulus equal to 90 MPa), current climate conditions, and road material properties. Then, the Mechanistic-Empirical Pavement Design Guide (MEPDG) was used to verify the response of the pavement structure. The fatigue verification of bound materials resulted in damage values much lower than 1 at the end of the 20-year service life (i.e., 0.12 with the Asphalt Institute and 0.31 with the Marchionna law, respectively) and highlights that the Italian catalogue's sheets are overdesigned. On the other hand, the rutting verification according to MEPDG is not satisfied after an 11-year service life (i.e., the total rutting is equal to 1.50 cm), forcing frequent and expensive maintenance of wearing and binder courses. Therefore, the results confirm the validity of the Italian catalogue for fatigue service life and suggest the need for high-performance asphalt to prevent early rutting due to bus traffic increasing by load and frequency in previous decades.

Keywords: bus lanes; bus fleet; pavement design catalogue; fatigue; rutting



Citation: Del Serrone, G.; Di Mascio, P.; Loprencipe, G.; Vita, L.; Moretti, L. Bus Lane Design Based on Actual Traffic Loads and Climate Conditions.

Infrastructures **2024**, *9*, 50.
<https://doi.org/10.3390/infrastructures9030050>

Academic Editor: Benedetto Barabino

Received: 7 February 2024

Revised: 2 March 2024

Accepted: 3 March 2024

Published: 5 March 2024



Copyright: © 2024 by the authors. Licensee MDPI, Basel, Switzerland. This article is an open access article distributed under the terms and conditions of the Creative Commons Attribution (CC BY) license (<https://creativecommons.org/licenses/by/4.0/>).

1. Introduction

A road pavement catalogue offers a simplified approach to design layer thicknesses based on traffic and subgrade bearing capacity related to the material characteristics. This tool is used worldwide for different pavements and infrastructures. In previous decades, solutions for airports [1], harbours [2], roads [3], and bike lanes [4] have been studied and proposed in the literature. Additionally, catalogues to design road pavements with recycled aggregates [5], modular pavements composed of cube stones [6], and concrete pavers have been published [7]. In Europe, many countries employ catalogues as official design methods to meet the needs of public administrations with easy- and prompt-to-use solutions. Germany uses a catalogue [8] to design pavements by varying traffic levels, subgrade bearing capacity, and frost susceptibility. This catalogue is updated every 10 years (most recently in 2012). Austria's bituminous pavement design and construction standard [9] provides solutions depending on daily average traffic and weather conditions. The French Technical Guide [10] suggests asphalt and concrete solutions based on material properties and pavement management. Croatia's national standard for asphalt pavement design [11] relies on the AASHO Road Test to design flexible structures. A new Polish catalogue for flexible and rigid pavements [12] updated traffic categories, materials, and technologies.

Pavement catalogues reflect long-term experience concerning materials' properties, climate conditions, and traffic levels. The mechanistic-empirical method, laboratory testing,

and field observations can validate the cross-sections proposed by catalogues [7,13,14]. In recent years, rational structural calculation methods have been implemented based on finite element analyses and fatigue laws [15]. Finite element methods (FEM) allow structural analysis of multi-layered pavement with specified mechanical characteristics [16–18]. However, they require high setting and computational time.

Since 1995, the Italian Pavement Design Catalogue [19] has been providing pre-calculated sets of pavement suitable for Italian traffic, climate conditions, and road types (i.e., rural highways, urban highways, primary rural and high-capacity roads, secondary rural roads, secondary touristic roads, high-speed urban roads, local roads, and bus lanes). It is the official design method for four pavement types (i.e., asphalt, semirigid, jointed plain concrete, and continuously reinforced concrete). For each road type, variety of boundary conditions in terms of subgrade bearing capacity (i.e., resilient modulus equal to 30 N/mm², 90 N/mm², and 150 N/mm²) and commercial traffic volume during the service life (i.e., 400,000, 1,500,000, 4,000,000, 10,000,000, 25,000,000, and 45,000,000), it gives four sheets, one for each pavement type. Not all combinations are reasonable for each road type, and it recommends more than 200 structural sections calculated with rigorous methods [20]. This design tool is used in the preliminary phases of a road project when the input parameters have not been investigated yet. Concerning bus lanes, it proposes 44 solutions. Figure 1 shows the sheet from the Italian catalogue for flexible bus lanes.

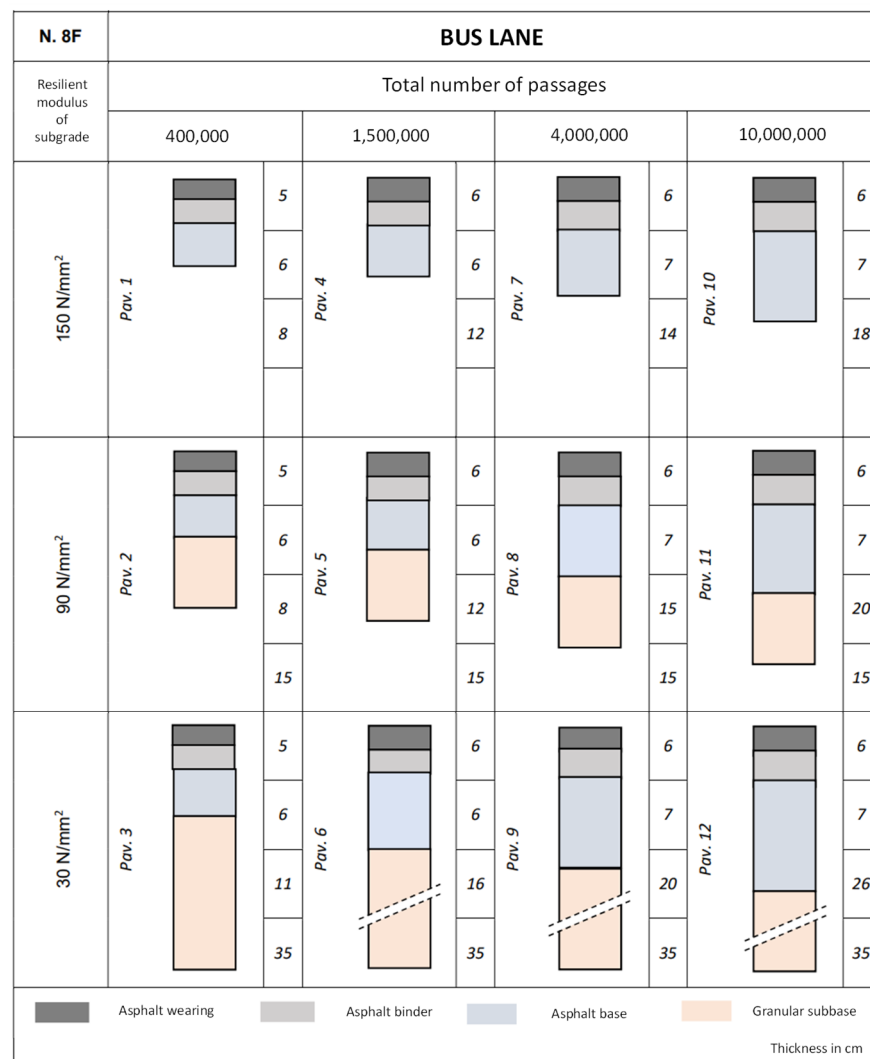


Figure 1. Bus lane designs for flexible pavements [19].

All the catalogue sheets show, in columns, the subgrade resilient modulus value in MPa, and in rows, the number of commercial vehicle passages (weight > 35 kN). As the resilient modulus increases, the deep layers (i.e., asphalt base and granular sub-base) can be reduced while the surface layers (i.e., wearing and binder courses) remain unchanged. Furthermore, as the number of heavy vehicle passages increases, the thicknesses of the all the asphalt layers increase.

In this study, four bus lanes in Rome, Italy, have been monitored hourly in 2022, in order to obtain the traffic mix and its daily, weekly, and seasonal distribution. The surveyed mix significantly differs from that proposed in the Italian catalogue and consists of two axle 12 m-long vehicles and three axle 18 m-long articulated vehicles, whose maximum weight is 195 kN and 305 kN, respectively.

The monitored traffic volume and spectrum, the actual subgrade bearing capacity, the catalogue climate conditions, and the road materials' properties have been used as input data to verify and compare the pavement of the busiest bus lane with the solution proposed by the Italian catalogue. Therefore, a stress-strain analysis has been performed, using KENLAYER software from the KENPAVE suite. This can calculate the pavement response structure based on the multilayer elastic response model [21]. The response in terms of stresses, strains, and deformations has been used for rutting according to MEPDG [22] and fatigue verification through the empirical prediction laws of the Marchionna and Asphalt Institute [20,23] over a 20-year service period.

This research provides a detailed examination of pavement performances, durability, and the prediction of its degradation over time. Specifically, it demonstrates that asphalt pavements, sized according to the Italian catalogue, have a satisfactory service life. Furthermore, they require repaving due to the formation of ruts, and anti-rutting mixtures are necessary to reduce resurfacing operations.

2. Materials and Methods

Figure 2 shows the procedure implemented in this study to verify the pavement in terms of fatigue and rutting under different input data. The presented flowchart is derived from the MEPDG methodology. It combines empirical elements and mechanical principles to calculate the pavement's response to varying layer materials (elastic modulus and Poisson ratio), traffic (loads spectra), climate (thermal seasonal variations), and sub-grade properties (bearing capacity).

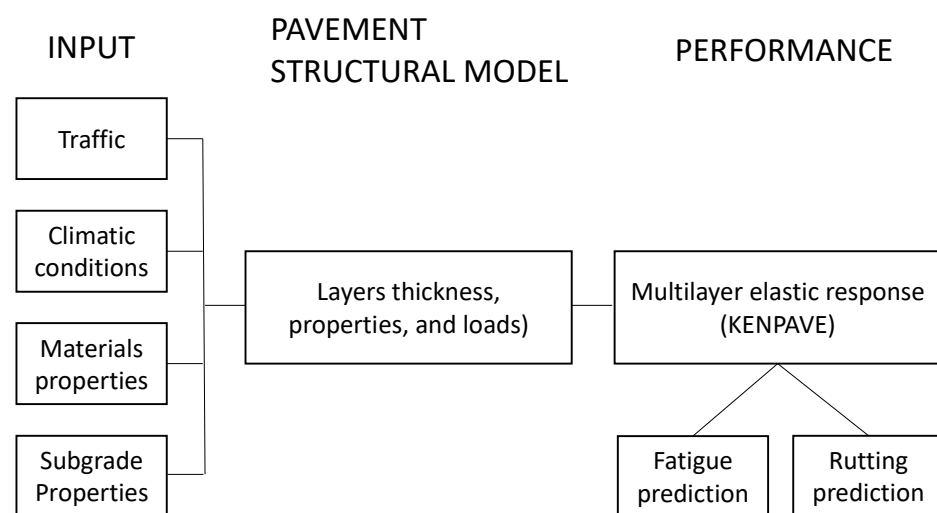


Figure 2. Applied methodology flowchart.

2.1. Traffic

Proper pavement design requires a thorough understanding of traffic flow, types of passing vehicles, and loads on the pavement. This study analysed the fleet of buses used in

the urban service of Rome (Italy) and the types of tourist buses passing through the bus lanes, looking for different overall masses, numbers, and types of axles compared to [19]. In recent years, Intelligent Transportation System (ITS) devices have provided innovative services for monitoring traffic in Rome [24]. The Mobility Control Centre has recorded the occupation of bus lanes through video surveillance cameras, allowing traffic data collection. Table 1 lists the most frequently detected bus models.

Table 1. Monitored bus models in Rome.

Vehicles for Urban Mass Transport	Vehicles for Tourist Transport
Iveco Irisbus Citelis 12 m	Setra Comfort Class 12 m
Iveco Irisbus Citelis 18 m	Mercedes-Benz Turismo 12 m
Iveco Urban Way 12 m	Man Lion’s Coach 12 m
Mercedes-Benz Citaro 12 m	
Temsa Avenue 12 m	

The weight and configuration of the axles do not differ between buses of the same length, while a considerable difference occurs between the 12 m-long and 18 m-long buses. In Table 2, the 12 m buses consist of two single axles (↓) of 75 (A) and 120 (B) kN, respectively, while the 18 m buses consist of three single axles of 75 (A), 110 (C) and 120 (B) kN, respectively. According to Table 1, Table 2 details the bus fleet assumed in this study and the weight of each individual axle is indicated by different letters.

Table 2. Actual urban bus fleet mix.

Vehicle Type	Illustration	Load Pattern	Axles Load ID and Weight (kN)
Bus 12 m			↓A (75) ↓B (120)
Bus 18 m (articulated bus)			↓A (75) ↓C (110) ↓B (120)

The actual urban bus fleet mix differs from the most widespread types of buses when the Italian CNR catalogue was drafted. Table 3 shows the bus fleet according to Italian CNR catalogue [19].

Table 3. Urban bus fleet according to Italian CNR catalogue [19].

Vehicle Type	Illustration	Load Pattern	Axles Load ID and Weight (kN)
Old Bus 1			↓D (40) ↓E (80)
Old Bus 2			↓F (60) ↓G (100)

All urban buses have two axles and weigh less than 160 kN (Table 3). By contrast, the new mix includes three axle vehicles that are 305 kN and two axle buses that are 195 kN. Given the collected mobility data, the modelled bus flow is composed of 80% 12 m-long and 20% 18 m-long buses.

The hourly seat-load factors of the vehicles have been investigated for accurate modelling of loads. Concerning the busiest month in the year, Figure 3 shows the average hourly distribution of traffic in one of the monitored bus lanes. The bars in Figure 3 distinguish tourist (i.e., orange bars) and public urban buses (i.e., blue bars).

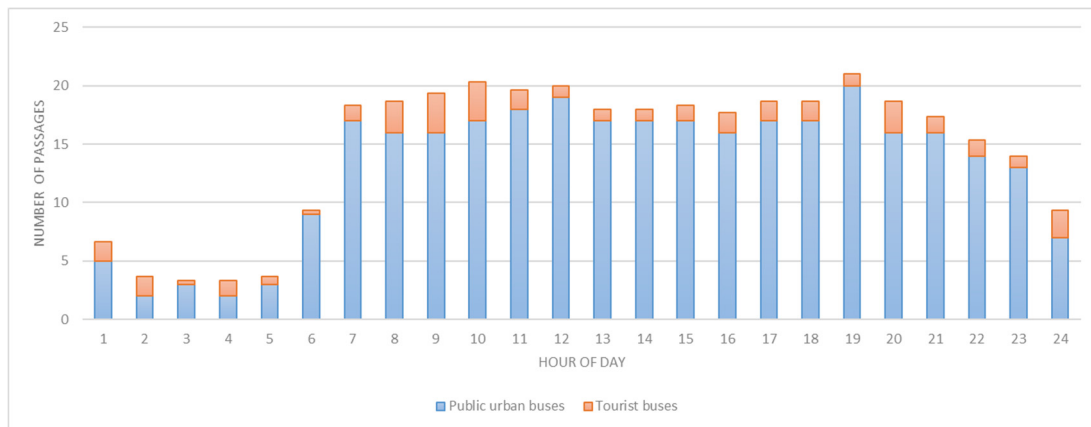


Figure 3. Public urban and tourist buses’ passages during a day in October 2022.

Tourist buses have a much lower frequency than city buses, over a 24 h period the share of tourist buses in relation to public urban buses is around 11%, therefore only public urban buses were considered in this study.

Finally, the hourly seat occupancy allowed a detailed analysis of stress-strain conditions by traffic. Table 4 shows the seat occupancy for the considered time slots.

Table 4. Bus seat occupancy in October 2022.

Time Slots	Seat Occupancy
6:00 a.m.–8:59 a.m.	100%
9:00 a.m.–11:59 a.m.	50%
12:00 p.m.–2:59 p.m.	70%
3:00 p.m.–5:59 p.m.	50%
6:00 p.m.–8:59 p.m.	100%
09:00 p.m.–5:59 a.m.	30%

Table 5 lists the curb and maximum weight of each bus model. Their difference gives the Gross Vehicle Weight, the sum of passengers, curb, and cargo weights.

Table 5. Axles’ maximum and curb weight for the actual studied bus fleet.

Bus Length	Axle ID	Maximum Weight (kN)	Curb Weight (kN)	Gross Vehicle Weight (kN)
12 m	A	75	44	31
	B	120	76	44
18 m	A	75	42	33
	C	110	66	44
	B	120	72	48

For each investigated bus lane (BL_i, $i = 1, \dots, 4$), Table 6 shows the monthly traffic volume in 2022.

Table 6. Investigated Bus Lanes (BL)—observed monthly traffic volume in 2022.

Season	Month	Number of Passages			
		BL1	BL2	BL3	BL4
Winter	January	18,684	18,643	10,066	10,704
	February	17,015	17,121	10,168	10,888
	March	19,360	19,380	10,738	11,212
Spring	April	18,339	18,228	10,194	10,482
	May	13,143	13,822	10,454	10,054
	June	12,544	11,345	10,322	9436

Table 6. *Cont.*

Season	Month	Number of Passages			
		BL1	BL2	BL3	BL4
Summer	July	11,252	10,244	9655	8710
	August	10,875	10,945	9435	8546
	September	17,126	17,422	10,788	9947
Autumn	October	19,835	19,856	11,064	10,727
	November	19,211	17,843	11,546	14,568
	December	19,586	18,517	11,455	12,075
	Total	196,970	193,366	125,885	127,349

Finally, the overall number of passages (y^N) after a 20-year service life (N) has been calculated according to Equation (1).

$$y^N = \sum_{n=1}^N y_1 \cdot (1 + r)^n \tag{1}$$

where y_1 is the traffic in the first year, n is the i -th year between 1 and N , and r is the yearly constant increasing rate equal to 0.5% according to [25]. Table 7 shows the expected number of passages of the surveyed BL i after 20 years.

Table 7. Investigated Bus Lanes (BL)—expected traffic 20-year service life.

Season	Month	Vehicles Passages			
		BL1	BL2	BL3	BL4
Winter	January	391,974	391,114	224,560	212,232
	February	356,960	359,183	213,316	214,382
	March	406,156	406,575	225,274	226,400
Spring	April	384,736	382,407	213,861	214,930
	May	275,729	289,973	219,316	220,412
	June	263,162	238,008	216,546	217,629
Summer	July	236,057	214,910	202,553	203,566
	August	228,148	229,616	197,938	198,928
	September	359,288	365,498	226,323	227,454
Autumn	October	416,121	416,561	232,113	233,273
	November	403,030	374,330	242,225	243,436
	December	410,897	388,470	240,316	241,517
	y^{20}	4,132,256	4,056,648	2,654,341	2654161

The maximum y^{20} is approximately 4 million cycles expected in 20 years, as shown in Table 7. For this reason, and because the 90 N/mm² is a typical Roman modulus of subgrade, pav. 8 was selected from the Italian catalogue for flexible bus lanes.

2.2. Climate Conditions

Since asphalt has thermosusceptible properties [26–28], the estimation of pavement temperature is pivotal to verifying pavements [29]. The thermal pavement conditions depend on climate inputs, the materials’ physical properties, and the layers’ thickness and depth [30]. The annual air temperatures in Rome were investigated through time series from the Italian Air Force data recorded over the last 20 years. Since no significant variations have been noted between the actual climatic conditions and those considered in the catalogue, this study used the climate conditions proposed by [31]. Table 8 lists average seasonal data in terms of air temperature (T), air temperature variation (T_V), solar irradiance (SI), and annual average wind speed (w).

Table 8. Italian CNR catalogue’s climatic conditions.

Season	Seasonal Average Air Temperature (T)	Seasonal Average Air Temperature Variation (T_V)	Seasonal Average Solar Irradiance (SI)	Annual Average Wind Speed (w)
	[°C]	[°C]	[kcal/m ²]	[km/h]
Winter	4.5	6.0	2718	13.00
Spring	11.5	7.5	5785	
Summer	22.0	10.6	6507	
Autumn	14.0	9.3	3547	

In this study, Barber’s law [32] has been adopted to estimate the layers’ temperature. Equation (2):

$$T_{pav}(z, t) = T + R + \left(\frac{T_v}{2} + 3R \right) \cdot F \cdot \exp(-C \cdot z) \cdot \sin \left(0.262t - C \cdot z - \arctan \frac{C}{H + C} \right), \quad (2)$$

where $T_{pav}(z, t)$ is the temperature in °C of the pavement at depth z and time t ; R is the daily solar radiation contribution to air temperature in °C, according to Equation (3):

$$R = \frac{2 \cdot b \cdot SI}{3 \cdot 24 \cdot h} \quad (3)$$

where b is the surface absorptivity for solar radiation; h is the surface coefficient according to Equation (4):

$$h = 4.882 \cdot \left(1.3 + 0.4332 \cdot w^{0.75} \right) \quad (4)$$

F is according to Equation (5):

$$F = \frac{H}{\sqrt{(H + C)^2 + C^2}} \quad (5)$$

H and C derive from Equations (6) and (7), respectively:

$$H = \frac{h}{p} \quad (6)$$

where p is the thermal conductivity and

$$C = \frac{0.131 \cdot s \cdot \gamma}{k} \quad (7)$$

where s is the specific heat, and γ is the bulk density.

Once all the parameters have been obtained, it is possible to determine the temperature at the midpoint of each asphalt layer by varying time and season.

2.3. Material Properties

The Witzak–Fonseca model [33] was used to model the mechanical performance of asphalt. This model was chosen due to its high accuracy. In this study [34], the authors estimated a coefficient of determination (R^2) of 0.88.

The complex stiffness modulus (E^*) depends on material temperature, loading speed, age, and physical characteristics of the mixture Equation (8):

$$E^* = 689 \times 10^a \quad (8)$$

where a is:

$$a = -0.261 + 0.008225 \cdot \rho_{200} - 0.00000101 \cdot (\rho_{200})^2 + 0.00196 \cdot \rho_4 - 0.03157 \cdot V_a - 0.415 \cdot \frac{V_{b\ eff}}{V_{b\ eff} + V_a} + \frac{1.87 + 0.002808 \cdot \rho_4 + 0.0000404 \cdot \rho_{\frac{3}{8}} - 0.0001786 \cdot (\rho_{\frac{3}{8}})^2 + 0.164 \cdot \rho_{\frac{3}{4}}}{1 + e^{(-0.716 \cdot \log(f) - 0.7425 \cdot \log(\frac{\eta}{10^6})}} \tag{9}$$

where η is the bitumen viscosity, f is the frequency of the load, V_a is the percentage of void content in the asphalt mixture, $V_{b\ eff}$ is the percentage of the effective bitumen content, $\rho_{3/4}$, $\rho_{3/8}$, and ρ_4 are the percentage of material retained on 3/4, 3/8, and 4 sieves, respectively, and ρ_{200} is the percentage passing a 200 sieve.

The viscosity of the unaged bitumen (η) can be derived from Equation (10) [22]:

$$\log \log \eta = A + VTS \log(1.8T + 491.68) \tag{10}$$

where T is the asphalt temperature in [°C]; A and VTS are dimensionless coefficients depending on the bitumen grade. These parameters have been identified for neat and modified aged bitumen [28,35,36]. Unlike the MEPDG method, this study calculates the modulus of elasticity of the mix using the A and VTS parameters for an already aged bitumen. Table 9 lists the reference values of A and VTS according to [37]:

Table 9. A and VTS coefficients for aged asphalt.

Coefficient	AC-20 (Wearing Course)	AC-10 (Binder Course)	AC-2.5 (Base Course)
A	10.9168	11.0770	11.8408
VTS	-3.6469	-3.7097	-3.9974

The aggregate size spectrum commonly used in Italy allowed the calculation of E^* for all asphalt layers by varying daily and seasonal temperatures (Figure 4).

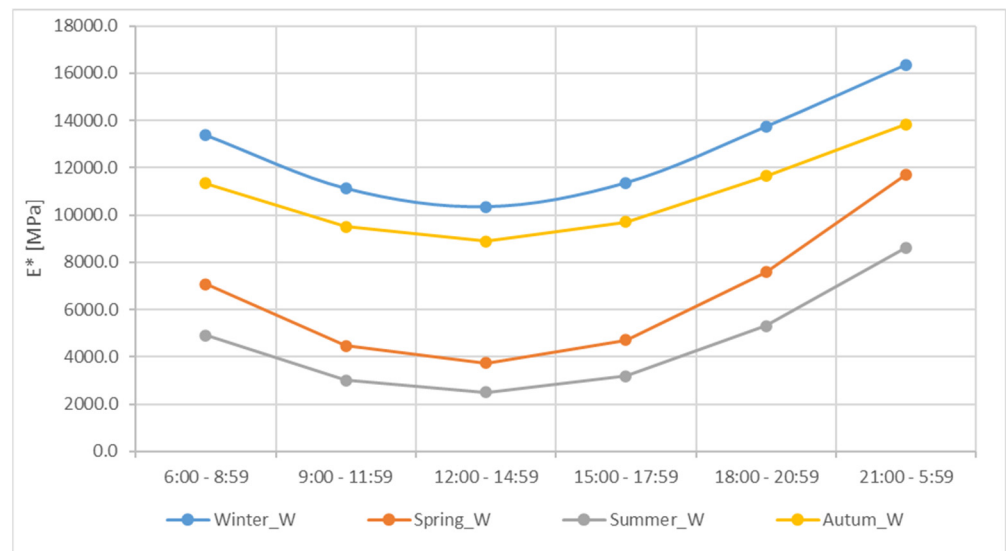


Figure 4. Daily and seasonal E^* curves for a wearing course.

The sub-base granular mix must have a minimum of 30% Californian Bearing Ratio, which equals 80 MPa resilient modulus according to [38,39]. Finally, a subgrade resilient module of 90 MPa has been chosen. Tables 10–13 list the asphalt’s complex moduli of each layer in winter, spring, summer, and autumn, respectively, used for pavement verification.

Table 10. Moduli of materials in the wintertime.

Layer	Winter Moduli (MPa)					
	6:00 a.m.–8:59 a.m.	9:00 a.m.–11:59 a.m.	12:00 p.m.–2:59 p.m.	3:00 p.m.–5:59 p.m.	6:00 p.m.–8:59 p.m.	9:00 p.m.–5:59 a.m.
Wearing	13,373	11,125	10,351	11,370	13,750	16,368
Binder	16,419	14,149	12,781	12,974	14,642	17,894
Base	16,733	15,696	14,512	13,864	14,093	16,108

Table 11. Moduli of materials in the springtime.

Layer	Spring Moduli (MPa)					
	6:00 a.m.–8:59 a.m.	9:00 a.m.–11:59 a.m.	12:00 p.m.–2:59 p.m.	3:00 p.m.–5:59 p.m.	6:00 p.m.–8:59 p.m.	9:00 p.m.–5:59 a.m.
Wearing	7081	4466	3741	4714	7594	11722
Binder	9125	6316	4926	5108	6873	11279
Base	9323	7955	6552	5854	6095	8483

Table 12. Moduli of materials in the summertime.

Layer	Summer Moduli (MPa)					
	6:00 a.m.–8:59 a.m.	9:00 a.m.–11:59 a.m.	12:00 p.m.–2:59 p.m.	3:00 p.m.–5:59 p.m.	6:00 p.m.–8:59 p.m.	9:00 p.m.–5:59 a.m.
Wearing	4909	3005	2500	3180	5299	8623
Binder	6249	4205	3240	3365	4601	7903
Base	6288	5290	4296	3815	3980	5671

Table 13. Moduli of materials in the autumntime.

Layer	Autumn Moduli (MPa)					
	6:00 a.m.–8:59 a.m.	9:00 a.m.–11:59 a.m.	12:00 p.m.–2:59 p.m.	3:00 p.m.–5:59 p.m.	6:00 p.m.–8:59 p.m.	9:00 p.m.–5:59 a.m.
Wearing	11,344	9515	8891	9713	11,654	13,843
Binder	13,675	11,850	10,761	10,914	12,244	14,878
Base	13,789	12,955	12,012	11,498	11,679	13,285

2.4. Pavement Structural Model

The input data have been used to assess stresses, deformations, and displacements in the designed road pavements through a specific calculation program based on the multilayered elastic theory [21]. The structural analyses focus on the interface between bound and unbound layers (e.g., asphalt subbase–subgrade and asphalt base–granular subbase, yellow points in Figure 5).

In the multilayer elastic theory, each axle load is usually symmetrical and equally distributed among the tires, and the tire load has a circular footprint area (green points in Figure 5) [6,40–42]. Figure 5a and b show the layouts from KENLAYER [43–45] of single and dual wheels, respectively, where the interface between layers is considered bonded and in full contact. The tire inflation pressure was equal to 750 kPa [46–48].

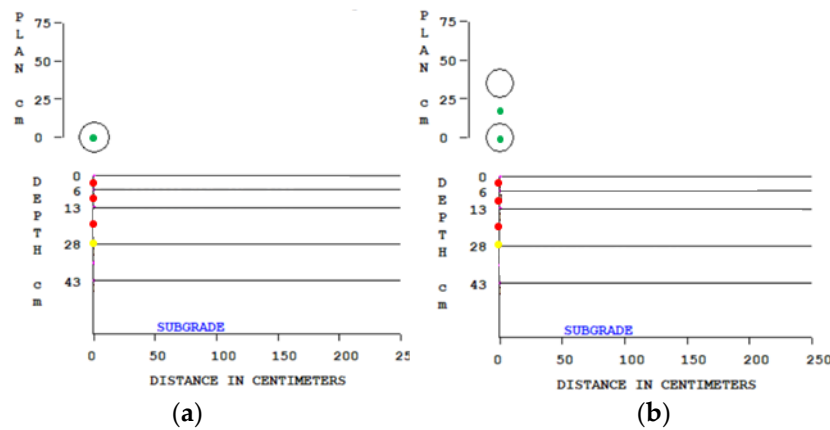


Figure 5. Loads and layers representation of (a) single-wheel load, and (b) dual-wheel load.

In Figure 5, green points in the top view are the positions where stresses and strains have been calculated. For the single-wheel axle, the point is the tire footprint centre because it is the most stressed position, while two points have been chosen for the dual-wheel axle (Figure 5b). It is crucial to select the most burdensome point at different depths. In the fatigue verification process, the most stressed point in the bonded layers is usually the deepest of the asphalt layers (the yellow point in Figure 5). For the rutting verification, it is necessary to evaluate the vertical deformation due to the vertical strain at the centre of each layer (i.e., the red points in Figure 5). KENLAYER outputs provide the pavement stress-strain conditions for each axle, time slot, and season used to verify fatigue and rutting.

2.5. Fatigue Cracking

Fatigue occurs in bonded layers due to cyclic tensile stresses due to vehicular traffic [49]. Miner’s law is the most used approach in calculating fatigue strength [50]. It assumes that the damage (D) caused by cyclic loads over time is cumulative and assigns to each passage a cumulative fatigue value, Equation (11).

$$D = \sum_{j=1}^4 \sum_{i=1}^5 \sum_{k=1}^6 \frac{n_{k,i,j}}{N_{f\ k,i,j}} \tag{11}$$

where k is the time slot, i is the axle weight, j is the season, $n_{k,i,j}$ is the predicted number of axle passages, and $N_{f\ k,i,j}$ is the maximum number of axles allowed according to the Marchionna [20] and Asphalt Institute [51–54] laws. Equation (12) was used to verify the Italian catalogue [19].

$$N_f = 10^{(6+4.7619 \cdot (\text{Log}(\frac{\Gamma \cdot V_b}{V_b + V_v}) - \text{Log} \epsilon_h))} + 1.373 \cdot e^{-1.098n} \cdot h_a^{(-0.157+0.476n)} \cdot \left[\left(\frac{|E^*|}{10} \right)^{\alpha'} \cdot \left(\frac{\sigma_h}{10} \right)^{\beta'} \cdot 10^{\mu'} \right] \tag{12}$$

where ϵ_h is the tensile strain at the bottom of the deepest asphalt layer; σ_h is the horizontal tensile stress at the bottom of the deepest asphalt layer; V_b is the volume of bitumen concerning the mixture; V_v is the air voids content; h_a is the height of the asphalt layers; Γ , n, α' , β' , and μ' are experimental coefficients.

Equation (13) shows the Asphalt Institute fatigue law:

$$N_f = A \cdot 0.00432 \cdot C \cdot \epsilon_h^{-3.291} \cdot |E^*|^{-0.854} \tag{13}$$

where A is equal to 18.4 [44]; C is a correction factor according to Equation (14):

$$C = 10^M \tag{14}$$

where $M = 4.84 \cdot \left(\frac{V_b}{V_a + V_b} - 0.69 \right)$

The stress-strain conditions have been analysed at the deepest point of the base layer because it is the bottom bound layer.

2.6. Rutting Law

Rutting is the accumulation of permanent vertical deformation due to the passage of vehicle tires (wheel path) in all or some of the layers in the pavement structure [55]. It affects both bound and unbound road materials. Traffic and environmental conditions cause rutting [56–58], and high temperatures make the mix more deformable and favourable to plastic deformations. In this study, the adopted rutting model complies with [22] Equation (15):

$$\epsilon_p = \epsilon_r \cdot K_1 \cdot 10^{K_2} \cdot (1.8 \cdot T + 32)^{K_3} \cdot (N)^B \tag{15}$$

where ϵ_p is the permanent strain after N load cycles, ϵ_r is the resilient strain obtained by elastic analysis, T is the temperature at the intermediate point of the layer calculated in this study with the Barber model, K_2 , K_3 , and B are the constant values -3.4488 , 1.5606 , and 0.4792 , respectively. Finally, K_1 is calculated according to Equations (16) to (18):

$$K_1 = \left(C_1 + \frac{C_2}{25.4} \cdot d \right) \cdot 0.328196^{\left(\frac{d}{25.4} \right)} \tag{16}$$

$$C_1 = 0.1039 \cdot \left(\frac{h_{ac}}{25.4} \right)^2 + 2.4868 \cdot \left(\frac{h_{ac}}{25.4} \right) - 17.342 \tag{17}$$

$$C_2 = 0.0172 \cdot \left(\frac{h_{ac}}{25.4} \right)^2 - 1.7331 \cdot \left(\frac{h_{ac}}{25.4} \right) + 27.428 \tag{18}$$

where h_{ac} is the thickness of the bitumen layers, and d is the calculation point depth.

Equation (15) is the model for permanent deformation under specific pavement conditions and load repetitions. The total rutting is not the sum of various contributions, but they are combined according to [22] (Figure 6):

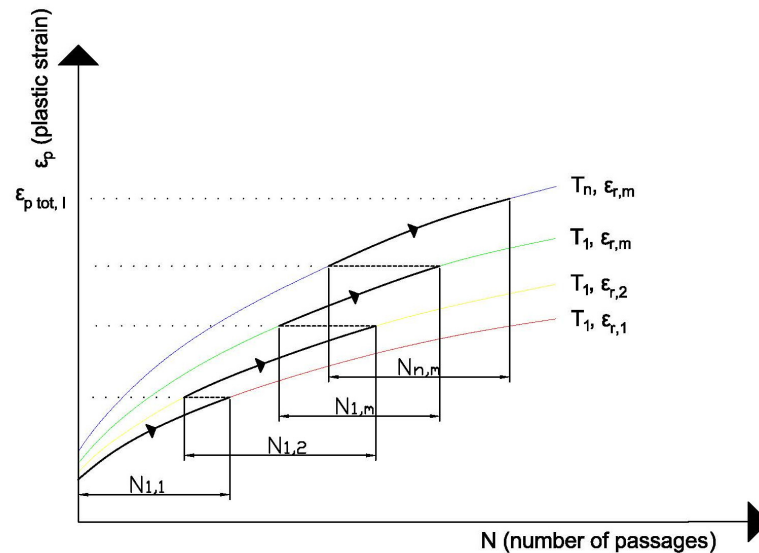


Figure 6. Combination of rutting phenomena based on MEPDG.

In Figure 6, $\epsilon_{p\ tot, l}$ is the permanent strain of the considered layer (l) according to Equation (19):

$$\epsilon_{p\ tot, l} = A_{n,m} \cdot \left(\sum_{j=1}^n \sum_{i=1}^m N_{i,j} \cdot \left(\frac{A_{i,j}}{A_{n,m}} \right)^{\frac{1}{B}} \right)^B \tag{19}$$

where j is the considered climate condition, n is the last climate condition, i is the load condition, m is the last axle, and A is a coefficient from Equation (20):

$$A = \epsilon_r \cdot K_1 \cdot 10^{K_2} \cdot (1.8 \cdot T + 32)^{K_3} \tag{20}$$

Finally, the overall deformation of the pavement (Δh) is according to Equation (21):

$$\Delta h = \sum_{l=1}^{tt} h_{a,l} \cdot \epsilon_{p,tot,l} \tag{21}$$

3. Results

The values of stresses and strains from the mechanical model allowed verifications of fatigue and rutting. Table 14 lists the horizontal outputs 28 cm below the pavement surface, where the bottom bound layer for fatigue verification is located.

Table 14. Horizontal stress-strain conditions ¹.

Season	Hour	Axle A (Single)		Axle B (Dual Wheel)		Axle C (Dual Wheel)	
		c (kPa)	ϵ_h (-)	σ_h (kPa)	ϵ_h (-)	σ_h (kPa)	ϵ_h (-)
Winter	6:00 a.m.–8:59 a.m.	−632.56	-2.96×10^{-5}	−845.59	-4.20×10^{-5}	−703.71	-3.51×10^{-5}
	9:00 a.m.–11:59 a.m.	−550.47	-2.75×10^{-5}	−710.83	-3.78×10^{-5}	−579.47	-3.09×10^{-5}
	12:00 a.m.–2:59 p.m.	−543.80	-2.94×10^{-5}	−700.10	-4.03×10^{-5}	−700.10	-4.03×10^{-5}
	3:00 p.m.–5:59 p.m.	−525.38	-2.97×10^{-5}	−677.28	-4.08×10^{-5}	−552.17	-3.34×10^{-5}
	6:00 p.m.–8:59 p.m.	−593.08	-3.30×10^{-5}	−791.29	-4.68×10^{-5}	−658.60	-3.90×10^{-5}
	9:00 p.m.–5:59 a.m.	−432.43	-2.10×10^{-5}	−545.77	-2.83×10^{-5}	−545.77	-2.83×10^{-5}
Spring	6:00 a.m.–8:59 a.m.	−576.25	-4.86×10^{-5}	−754.45	-6.79×10^{-5}	−628.31	-5.67×10^{-5}
	9:00 a.m.–11:59 a.m.	−510.63	-5.05×10^{-5}	−638.96	-6.80×10^{-5}	−521.34	-5.56×10^{-5}
	12:00 a.m.–2:59 p.m.	−492.11	-5.92×10^{-5}	−609.74	-7.91×10^{-5}	−609.74	-7.91×10^{-5}
	3:00 p.m.–5:59 p.m.	−451.36	-6.08×10^{-5}	−561.14	-8.15×10^{-5}	−457.96	-6.66×10^{-5}
	6:00 p.m.–8:59 p.m.	−486.26	-6.29×10^{-5}	−632.75	-8.76×10^{-5}	−527.13	-7.31×10^{-5}
	9:00 p.m.–5:59 a.m.	−364.24	-3.38×10^{-5}	−453.83	-4.50×10^{-5}	−453.83	-4.50×10^{-5}
Summer	6:00 a.m.–8:59 a.m.	−530.57	-6.65×10^{-5}	−664.72	-8.78×10^{-5}	−557.63	-7.36×10^{-5}
	9:00 a.m.–11:59 a.m.	−468.50	-6.99×10^{-5}	−563.85	-8.89×10^{-5}	−463.72	-7.31×10^{-5}
	12:00 a.m.–2:59 p.m.	−447.20	-8.24×10^{-5}	−532.34	-1.04×10^{-4}	−532.34	-1.04×10^{-4}
	3:00 p.m.–5:59 p.m.	−407.75	-8.47×10^{-5}	−486.40	-1.07×10^{-4}	−400.13	-8.79×10^{-5}
	6:00 p.m.–8:59 p.m.	−437.84	-8.71×10^{-5}	−543.01	-1.14×10^{-4}	−455.63	-9.57×10^{-5}
	9:00 p.m.–5:59 a.m.	−330.79	-4.60×10^{-5}	−399.05	-5.84×10^{-5}	−399.05	-5.84×10^{-5}
Autumn	6:00 a.m.–8:59 a.m.	−609.31	-3.47×10^{-5}	−788.78	-4.70×10^{-5}	−660.68	-3.94×10^{-5}
	9:00 a.m.–11:59 a.m.	−529.55	-3.21×10^{-5}	−666.34	-4.23×10^{-5}	−546.82	-3.47×10^{-5}
	12:00 a.m.–2:59 p.m.	−522.88	-3.42×10^{-5}	−655.83	-4.49×10^{-5}	−655.83	-4.49×10^{-5}
	3:00 p.m.–5:59 p.m.	−505.98	-3.45×10^{-5}	−635.13	-4.55×10^{-5}	−521.25	-3.73×10^{-5}
	6:00 p.m.–8:59 p.m.	−571.98	-3.84×10^{-5}	−738.17	-5.20×10^{-5}	−618.34	-4.35×10^{-5}
	9:00 p.m.–5:59 a.m.	−417.30	-2.46×10^{-5}	−515.59	-3.19×10^{-5}	−515.59	-3.19×10^{-5}

¹ negative values are traction stresses and extension strains.

The decrease in E^* due to the asphalt temperature decreases stress and increases strain (Tables 10–13). For each axle and time slot, the summer strain is about 140% higher than in winter and 70% higher than in spring or autumn. For example, ϵ_h of axle B in the late evening is -4.68×10^{-5} in winter and -1.14×10^{-4} in summer. According to Table 2, the modelled dual wheel axles weigh about 60% more than the single ones, but their increase in stress is about 25%. Comparing the A and B axles, the stress increase is at its maximum during wintertime (i.e., -632.56 kPa vs. -845.59 kPa at 6:00 a.m.–8:59 a.m.) and minimum during summertime (i.e., -447.20 kPa vs. -532.34 kPa at 12:00 p.m.–2:59 p.m.). The results in Table 14 allowed for the fatigue damage calculation reported in Table 15.

Table 15. Fatigue damage calculation according to Equation (11).

Season	Hour	Axle A (Single)		Axle B (Dual Wheel)		Axle C (Dual Wheel)	
		Marchionna Law	Asphalt Institute	Marchionna Law	Asphalt Institute	Marchionna Law	Asphalt Institute
Winter	6:00 a.m.–8:59 a.m.	5.94×10^{-4}	5.00×10^{-4}	1.49×10^{-4}	1.25×10^{-4}	2.78×10^{-4}	2.18×10^{-4}
	9:00 a.m.–11:59 a.m.	4.17×10^{-4}	3.37×10^{-4}	4.96×10^{-5}	4.79×10^{-5}	1.60×10^{-4}	1.24×10^{-4}
	12:00 a.m.–2:59 p.m.	5.47×10^{-4}	3.89×10^{-4}	1.37×10^{-4}	9.72×10^{-5}	4.60×10^{-4}	2.76×10^{-4}
	3:00 p.m.–5:59 p.m.	5.52×10^{-4}	4.01×10^{-4}	6.70×10^{-5}	5.71×10^{-5}	2.06×10^{-4}	1.47×10^{-4}
	6:00 p.m.–8:59 p.m.	7.20×10^{-4}	5.39×10^{-4}	1.80×10^{-4}	1.35×10^{-4}	3.18×10^{-4}	2.34×10^{-4}
	9:00 p.m.–5:59 a.m.	7.53×10^{-5}	9.73×10^{-5}	1.88×10^{-5}	2.43×10^{-5}	6.20×10^{-5}	6.42×10^{-5}
Spring	6:00 a.m.–8:59 a.m.	2.84×10^{-3}	1.19×10^{-3}	7.11×10^{-4}	2.97×10^{-4}	1.00×10^{-4}	4.94×10^{-4}
	9:00 a.m.–11:59 a.m.	3.35×10^{-3}	1.01×10^{-3}	4.43×10^{-4}	1.45×10^{-4}	1.03×10^{-3}	3.47×10^{-4}
	12:00 a.m.–2:59 p.m.	5.55×10^{-3}	1.42×10^{-3}	1.39×10^{-3}	3.56×10^{-4}	3.14×10^{-3}	9.23×10^{-4}
	3:00 p.m.–5:59 p.m.	4.94×10^{-3}	1.53×10^{-3}	6.87×10^{-4}	2.19×10^{-4}	1.40×10^{-3}	5.16×10^{-4}
	6:00 p.m.–8:59 p.m.	3.75×10^{-3}	1.82×10^{-3}	9.37×10^{-4}	4.55×10^{-4}	1.28×10^{-3}	7.47×10^{-4}
	9:00 p.m.–5:59 a.m.	3.10×10^{-4}	2.31×10^{-4}	7.74×10^{-5}	5.77×10^{-5}	1.89×10^{-4}	1.48×10^{-4}
Summer	6:00 a.m.–8:59 a.m.	6.22×10^{-3}	2.11×10^{-3}	1.56×10^{-3}	5.28×10^{-4}	1.92×10^{-3}	7.37×10^{-4}
	9:00 a.m.–11:59 a.m.	7.73×10^{-3}	1.83×10^{-3}	1.09×10^{-3}	2.63×10^{-4}	1.97×10^{-3}	5.30×10^{-4}
	12:00 a.m.–2:59 p.m.	1.20×10^{-2}	2.59×10^{-3}	3.00×10^{-3}	6.48×10^{-4}	5.40×10^{-3}	1.39×10^{-3}
	3:00 p.m.–5:59 p.m.	9.97×10^{-3}	2.80×10^{-3}	1.46×10^{-3}	4.02×10^{-4}	2.41×10^{-3}	7.90×10^{-4}
	6:00 p.m.–8:59 p.m.	6.86×10^{-3}	3.32×10^{-3}	1.72×10^{-3}	8.31×10^{-4}	1.97×10^{-3}	1.13×10^{-3}
	9:00 p.m.–5:59 a.m.	6.37×10^{-4}	4.13×10^{-4}	1.59×10^{-4}	1.03×10^{-4}	3.07×10^{-4}	2.26×10^{-4}
Autumn	6:00 a.m.–8:59 a.m.	1.15×10^{-3}	7.54×10^{-4}	2.70×10^{-4}	1.77×10^{-4}	4.19×10^{-4}	2.69×10^{-4}
	9:00 a.m.–11:59 a.m.	8.09×10^{-4}	5.04×10^{-4}	9.30×10^{-5}	6.74×10^{-5}	2.48×10^{-4}	1.54×10^{-4}
	12:00 a.m.–2:59 p.m.	1.03×10^{-3}	5.78×10^{-4}	2.43×10^{-4}	1.36×10^{-4}	6.62×10^{-4}	3.34×10^{-4}
	3:00 p.m.–5:59 p.m.	1.03×10^{-3}	5.96×10^{-4}	1.21×10^{-4}	7.97×10^{-5}	3.07×10^{-4}	1.80×10^{-4}
	6:00 p.m.–8:59 p.m.	1.31×10^{-3}	8.05×10^{-4}	3.08×10^{-4}	1.89×10^{-4}	4.57×10^{-4}	2.85×10^{-4}
	9:00 p.m.–5:59 a.m.	1.52×10^{-4}	1.47×10^{-4}	3.56×10^{-5}	3.46×10^{-5}	9.67×10^{-5}	8.06×10^{-5}

Summer is the most severe season for fatigue despite its low traffic volume (Table 7), due to a decrease in the elastic complex modulus. Table 16 summarises the fatigue damage calculation at the end of the service life. Both laws verify pav. 8 in Figure 1. Despite the new traffic mix, pav. 8 is still satisfactory with fatigue.

Table 16. Fatigue verification results.

Fatigue Law	Winter	Spring	Summer	Autumn	D
Marchionna Equation (12)	0.02	0.09	0.17	0.03	0.31
Asphalt Institute Equation (13)	0.01	0.04	0.06	0.02	0.12

Marchionna’s fatigue law is more severe than the Asphalt Institute one (i.e., D is 0.31 vs. 0.12). Their approach to fatigue threshold can explain such differences. The fatigue threshold is 10% fatigue cracking in the wheel path according to Marchionna’s law [20] and 20% according to the Asphalt Institute law [53,59,60].

Finally, rutting has been verified from vertical strain in the middle point of each layer. Table 17 lists the vertical stress-strain conditions of the wearing layer, which is the most critical one.

In Table 17, the highest strain occurs during summer (e.g., at 9:00 a.m.–11:59 a.m. the strain values are 4.56×10^{-5} in wintertime and 2.04×10^{-4} in summertime for the A axle). It reveals that summer has the highest rutting incidence despite having the lowest traffic volume.

Table 17. Vertical stress-strain conditions ¹.

Season	Hour	Axle A (Single)		Axle B (Dual Wheel)		Axle C (Dual Wheel)	
		σ_v (kPa)	ϵ_v (-)	σ_v (kPa)	ϵ_v (-)	σ_v (kPa)	ϵ_v (-)
Winter	6:00 a.m.–8:59 a.m.	736.753	3.53×10^{-5}	735.130	3.22×10^{-5}	732.638	3.48×10^{-5}
	9:00 a.m.–11:59 a.m.	737.014	4.56×10^{-5}	734.423	4.30×10^{-5}	731.064	4.58×10^{-5}
	12:00 a.m.–2:59 p.m.	736.746	4.91×10^{-5}	733.986	4.64×10^{-5}	733.986	4.64×10^{-5}
	3:00 p.m.–5:59 p.m.	734.498	4.38×10^{-5}	731.382	4.12×10^{-5}	727.459	4.40×10^{-5}
	6:00 p.m.–8:59 p.m.	733.733	3.33×10^{-5}	731.527	3.02×10^{-5}	728.342	3.28×10^{-5}
	9:00 p.m.–5:59 a.m.	728.347	3.08×10^{-5}	724.213	2.93×10^{-5}	724.212	2.93×10^{-5}
Spring	6:00 a.m.–8:59 a.m.	737.686	6.96×10^{-5}	736.305	6.53×10^{-5}	734.001	6.95×10^{-5}
	9:00 a.m.–11:59 a.m.	740.455	1.21×10^{-4}	738.317	1.17×10^{-4}	735.765	1.22×10^{-4}
	12:00 a.m.–2:59 p.m.	739.865	1.45×10^{-4}	737.348	1.40×10^{-4}	737.348	1.40×10^{-4}
	3:00 p.m.–5:59 p.m.	734.567	1.10×10^{-4}	731.160	1.06×10^{-4}	726.817	1.12×10^{-4}
	6:00 p.m.–8:59 p.m.	729.902	6.09×10^{-5}	727.035	5.65×10^{-5}	722.969	6.08×10^{-5}
	9:00 p.m.–5:59 a.m.	722.495	4.23×10^{-5}	717.893	4.05×10^{-5}	717.893	4.05×10^{-5}
Summer	6:00 a.m.–8:59 a.m.	737.585	1.19×10^{-4}	736.116	1.15×10^{-4}	733.65	1.19×10^{-4}
	9:00 a.m.–11:59 a.m.	740.401	2.04×10^{-4}	738.110	2.01×10^{-4}	735.335	2.06×10^{-4}
	12:00 a.m.–2:59 p.m.	739.644	2.46×10^{-4}	736.976	2.42×10^{-4}	736.976	2.42×10^{-4}
	3:00 p.m.–5:59 p.m.	734.068	1.88×10^{-4}	730.546	1.84×10^{-4}	726.017	1.89×10^{-4}
	6:00 p.m.–8:59 p.m.	729.032	1.05×10^{-4}	726.054	1.01×10^{-4}	721.780	1.05×10^{-4}
	9:00 p.m.–5:59 a.m.	720.766	6.65×10^{-5}	715.980	6.50×10^{-5}	715.980	6.50×10^{-5}
Autumn	6:00 a.m.–8:59 a.m.	736.379	4.19×10^{-5}	734.698	3.84×10^{-5}	732.105	4.14×10^{-5}
	9:00 a.m.–11:59 a.m.	736.489	5.35×10^{-5}	733.816	5.07×10^{-5}	730.343	5.39×10^{-5}
	12:00 a.m.–2:59 p.m.	736.204	5.73×10^{-5}	733.372	5.44×10^{-5}	733.372	5.44×10^{-5}
	3:00 p.m.–5:59 p.m.	734.046	5.15×10^{-5}	730.878	4.86×10^{-5}	726.871	5.18×10^{-5}
	6:00 p.m.–8:59 p.m.	733.429	3.97×10^{-5}	731.177	3.62×10^{-5}	727.916	3.92×10^{-5}
	9:00 p.m.–5:59 a.m.	727.815	3.66×10^{-5}	723.605	3.49×10^{-5}	723.605	3.49×10^{-5}

¹ negative values are traction stresses and extension strains.

According to Equation (21), Table 18 shows the rut depth evolution for the wearing and binder courses. The sum of the two contributions is the total rut depth.

Table 18. Rutting evolution.

Year	$\Delta h_{\text{Wearing course}}$ (cm)	$\Delta h_{\text{binder course}}$ (cm)	$\Delta h_{\text{base course}}$ (cm)	Δh_{Total} (cm)
1	0.34	0.13	0.00	0.47
2	0.48	0.18	0.00	0.66
3	0.58	0.22	0.00	0.80
4	0.67	0.25	0.00	0.92
5	0.75	0.28	0.00	1.03
6	0.81	0.31	0.00	1.12
7	0.88	0.33	0.00	1.21
8	0.94	0.36	0.00	1.30
9	0.98	0.38	0.00	1.36
10	1.05	0.40	0.00	1.45
11	1.10	0.42	0.00	1.52
12	1.14	0.43	0.00	1.57
13	1.19	0.45	0.00	1.64
14	1.23	0.47	0.00	1.70
15	1.28	0.48	0.00	1.76
16	1.32	0.50	0.00	1.82
17	1.36	0.52	0.00	1.88
18	1.40	0.53	0.00	1.93
19	1.44	0.55	0.00	1.99
20	1.48	0.56	0.00	2.04

Rutting exceeds the limit of 1.5 cm in the 11th year [52,53], so it is not verified throughout the life of the pavement, and it is necessary to anticipate the rehabilitation of the wearing and binder courses.

4. Conclusions

Over the last 20 years, we have seen an increase in commercial vehicles' mass, which can affect the durability and life of the pavement, so it is necessary to review the input data to discover a more correct design. In 2022, data from traffic monitoring systems have been collected from four bus lanes in Rome to verify flexible pavements. A network of ITS (Intelligent Transport System) sensors returned the traffic mix and traffic level, allowing detailed modelling of the load distribution over the year. Thanks to the ITS system and the traffic growth trends, it was possible to identify a range between 2.6 and 4 million passages during a 20-year service life. This analysis also included a detailed observation of the traffic spectrum, specifically focusing on buses that are 12 and 18 m in length. Dual wheel buses are the major difference between the current traffic mix and the traffic mix considered in the Italian catalogue to design pavements of bus lanes. This axle configuration favours pavement structures because the induced stresses do not increase proportionally, despite the axle weight.

The hourly traffic of the busiest lane and weather data allowed a sophisticated analysis of the asphalt complex modulus to predict fatigue and rutting according to experimental laws in the literature. Stresses and strains in the pavement are identified using KEN-LAYER according to the multilayered elastic theory, which is a valid tool for verifying road pavements.

The seasonal analysis of the cumulative fatigue damage showed that despite the lower number of passages during the summer, the cumulative damage is higher due to the decrease in stiffness and the increase in deformations. These factors contribute to a decrease in pavement life. The prediction results depend on the adopted fatigue law. The results of this study show that the analysed pavement has fatigue damage $D = 0.31$ for the Marchionna law and $D = 0.12$ for the Asphalt Institute law at the end of its service life.

The results of the study show that the pavement catalogue has a higher safety factor because the pavement continues to have a long service life despite increasing loads. Therefore, it is important to verify that the catalogue is used with appropriate design methods and actual field conditions. Nevertheless, rutting reaches 2.1 cm, which is more than the admitted limit (i.e., 1.5 cm), and it requires the resurfacing of wearing and binder courses every 10 years. It suggests high-performance mixtures to reduce the rutting rate, maintenance costs, and environmental impacts.

The results of this research are valuable for conducting feasibility analyses and initial evaluations of the pavement management system. A catalogue provides engineers with a basis for early estimation of construction and maintenance costs and materials required for the infrastructure. However, these results are affected by the input data; detailed studies of traffic, sub-grade strength, and climatic conditions, which are essential for application under different conditions. A sensitivity analysis could identify a range of climatic, traffic, and pavement conditions that would validate the fatigue and rutting assessments.

Author Contributions: Conceptualization, P.D.M. and G.L.; methodology, L.M.; software, L.V.; validation, L.M. and G.D.S.; formal analysis, P.D.M.; investigation, G.L. and L.V.; data curation, G.D.S.; writing—original draft preparation, L.M. and G.D.S.; writing—review and editing, L.V. and L.M.; supervision, G.L.; project administration, P.D.M. All authors have read and agreed to the published version of the manuscript.

Funding: This research received no external funding.

Data Availability Statement: Data are contained within the article.

Acknowledgments: The authors thank Salvatore Bruno for his contributions.

Conflicts of Interest: The authors declare no conflicts of interest.

References

- Di Mascio, P.; De Rubeis, A.; De Marchis, C.; Germinario, A.; Metta, G.; Salzillo, R.; Moretti, L. Jointed Plain Concrete Pavements in Airports: Structural–Economic Evaluation and Proposal for a Catalogue. *Infrastructures* **2021**, *6*, 73. [CrossRef]
- Barber, S.D.; Knapton, J. Structural Design of Block Pavements for Ports. *Concr. Block Paving* **2011**, *1*, 141–149.
- Saudy, M.; Breakah, T.; El-Badawy, S.; Khedr, S. Development of a Flexible Pavement Design Catalogue Based on Mechanistic–Empirical Pavement Design Approach: Egyptian Case Study. *Innov. Infrastruct. Solut.* **2021**, *6*, 206. [CrossRef]
- Tavira, J.; Jiménez, J.R.; Ayuso, J.; López-Uceda, A.; Ledesma, E.F. Recycling Screening Waste and Recycled Mixed Aggregates from Construction and Demolition Waste in Paved Bike Lanes. *J. Clean. Prod.* **2018**, *190*, 211–220. [CrossRef]
- Barbudo, A.; Jiménez, J.R.; Ayuso, J.; Galvín, A.P.; Agrela, F. Catalogue of Pavements with Recycled Aggregates from Construction and Demolition Waste. *Proceedings* **2018**, *2*, 1282. [CrossRef]
- Colagrande, S.; Quresima, R. Natural Cube Stone Road Pavements: Design Approach and Analysis. *Transp. Res. Procedia* **2023**, *69*, 37–44. [CrossRef]
- Di Mascio, P.; Moretti, L.; Capannolo, A. Concrete Block Pavements in Urban and Local Roads: Analysis of Stress-Strain Condition and Proposal for a Catalogue. *J. Traffic Transp. Eng. Engl. Ed.* **2019**, *6*, 557–566. [CrossRef]
- Richtlinien Für Die Standardisierung Des Oberbaus von Verkehrsflächen: RStO 12*; Forschungsgesellschaft für Straßen- und Verkehrswesen, Ed.; FGSV; Forschungsges. für Strassen- und Verkehrswesen: Köln, Germany, 2012; ISBN 978-3-86446-021-0.
- Blab, R.; Eberhardsteiner, L. Neuer Oberbaukatalog Für Straßenaufbauten—RVS 03.08.63. *Straße Autob.* **2016**, *67*, 933–935.
- Corté, J.-F.; Goux, M.-T. Design of Pavement Structures: The French Technical Guide. *Transp. Res. Rec.* **1996**, *1539*, 116–124. [CrossRef]
- Vukobratović, N.; Barišić, I.; Josip Juraj Strossmayer University of Osijek, Faculty of Civil Engineering Osijek; Dimter, S. Analyses of the Influence of Material Characteristics on Pavement Design. *Elektron. Časopis Građev. Fak. Osijek* **2017**, *8*, 8–19. [CrossRef]
- Judycki, J.; Jaskała, P.; Pyszczola, M.; Ryś, D.; Jaczewski, M.; Alenowicz, J.; Dołżycki, B.; Stienss, M. New Polish Catalogue of Typical Flexible and Semi-Rigid Pavements. *MATEC Web. Conf.* **2017**, *122*, 04002. [CrossRef]
- Hall, K. *Long-Life Concrete Pavements in Europe and Canada*; US Department of Transportation: Washington, DC, USA, 2007.
- Di Mascio, P.; Loprencipe, G.; Cantisani, G. Global Assessment Method of Road Distresses. *Life-Cycle Struct. Syst.* **2015**, *4*, 1113–1120. [CrossRef]
- Subagio, B.S.; Prayoga, A.B.; Fadilah, S.R. Implementation of Mechanistic–Empirical Pavement Design Guide against Indonesian Conditions Using Arizona Calibration. *Open Civ. Eng. J.* **2022**, *16*, e187414952210251. [CrossRef]
- Maina, J.W.; Denneman, E.; De Beer, M. Introduction of New Road Pavement Response Modelling Software by Means of Benchmarking. In Proceedings of the 27th Annual Southern African Transport Conference 2008, Pretoria, South Africa, 7–11 July 2008.
- Karadag, H.; Firat, S.; Isik, N.S.; Yilmaz, G. Determination of Permanent Deformation of Flexible Pavements Using Finite Element Model. *Građevinar* **2022**, *74*, 471–480.
- Awosanya, D.O.; Murana, A.A.; Olowosulu, A.T. Mechanistic–Empirical Flexible Pavement Analysis Using Load Spectra. *FUOYE J. Eng. Technol.* **2023**, *8*, 508–514. [CrossRef]
- CNR. Catalogo delle Pavimentazioni Stradali I, B.U. n. 178 Parte IV—Norme Tecniche. Consiglio Nazionale delle Ricerche: Roma, Italy, 1995. (In Italian)
- Marchionna, A.; Cesarini, M.; Fornaci, M.G.; Malgarini, M. Modello Di Degradazione Strutturale Delle Pavimentazioni. *Autostrade* **1985**, *1*, 85.
- Burmister, D. The General Theory of Stresses and Displacements in Layered Systems. I. *J. Appl. Phys.* **1945**, *16*, 89–94. [CrossRef]
- Mechanistic–Empirical Pavement Design Guide: A Manual of Practice*; Interim ed.; American Association of State Highway and Transportation Officials: Washington, DC, USA, 2011; ISBN 978-1-56051-423-7.
- Behiry, A.E.A.E.-M. Fatigue and Rutting Lives in Flexible Pavement. *Ain Shams Eng. J.* **2012**, *3*, 367–374. [CrossRef]
- Brinchi, S.; Carrese, S.; Cipriani, E.; Colombaroni, C.; Crisalli, U.; Fusco, G.; Gemma, A.; Isaenko, N.; Mannini, L.; Petrelli, M. COVID-19 Transport Analytics: Analysis of Rome Mobility During Coronavirus Pandemic Era. In *Proceedings of the Advances in Mobility-as-a-Service Systems*; Nathanail, E.G., Adamos, G., Karakikes, I., Eds.; Springer International Publishing: Cham, Switzerland, 2021; pp. 1045–1055.
- S.T.A.T.U.S. | Roma Mobilità. Available online: <https://romamobilita.it/it/progetti/studi-indagini/status> (accessed on 28 June 2023).
- Adwan, I.; Milad, A.; Memon, Z.A.; Widyatmoko, I.; Ahmat Zanuri, N.; Memon, N.A.; Yusoff, N.I.M. Asphalt Pavement Temperature Prediction Models: A Review. *Appl. Sci.* **2021**, *11*, 3794. [CrossRef]
- Fiore, N.; Bruno, S.; Del Serrone, G.; Iacobini, F.; Giorgi, G.; Rinaldi, A.; Moretti, L.; Duranti, G.M.; Peluso, P.; Vita, L.; et al. Experimental Analysis of Hot-Mix Asphalt (HMA) Mixtures with Reclaimed Asphalt Pavement (RAP) in Railway Sub-Ballast. *Materials* **2023**, *16*, 1335. [CrossRef]
- Rasmussen, R.O.; Lytton, R.L.; Chang, G.K. Method to Predict Temperature Susceptibility of an Asphalt Binder. *J. Mater. Civ. Eng.* **2002**, *14*, 246–252. [CrossRef]
- Gunka, V.; Demchuk, Y.; Sidun, I.; Miroshnichenko, D.; Nyakuma, B.B.; Pyshyev, S. Application of Phenol-Cresol-Formaldehyde Resin as an Adhesion Promoter for Bitumen and Asphalt Concrete. *Road Mater. Pavement Des.* **2021**, *22*, 2906–2918. [CrossRef]
- Laurinavičius, A.; Džygys, D. Thermal Conditions of Road Pavements and Their Influence on Motor Traffic. *Transport* **2003**, *18*, 23–31. [CrossRef]

31. Consiglio Nazionale delle Ricerche. Catalogo delle Pavimentazioni Stradali. In *Consiglio Nazionale delle Ricerche, Bollettino Ufficiale*; Terra, M., Ed.; Consiglio Nazionale delle Ricerche: Rome, Italy, 1995; Volume 178, p. 95. (In Italian)
32. Barber, E.S. Calculation of Maximum Pavement Temperatures from Weather Reports. *Highw. Res. Board Bull.* **1957**, *168*, 00237705.
33. Witczak, M.W.; Fonseca, O.A. Revised Predictive Model for Dynamic (Complex) Modulus of Asphalt Mixtures. *Transp. Res. Rec.* **1996**, *1540*, 15–23. [[CrossRef](#)]
34. Khattab, A.M.; El-Badawy, S.M.; Al Hazmi, A.A.; Elmwafi, M. Evaluation of Witczak E* Predictive Models for the Implementation of AASHTOWare-Pavement ME Design in the Kingdom of Saudi Arabia. *Constr. Build. Mater.* **2014**, *64*, 360–369. [[CrossRef](#)]
35. Griffith, J.M.; Puzinauskas, V.P. *Relation of Empirical Tests to Fundamental Viscosity of Asphalt Cement*; ASTM International: West Conshohocken, PA, USA, 1963.
36. Owais, M.; Moussa, G.S. Global Sensitivity Analysis for Studying Hot-Mix Asphalt Dynamic Modulus Parameters. *Constr. Build. Mater.* **2024**, *413*, 134775. [[CrossRef](#)]
37. Fernando, E.G.; Liu, W. *User's Guide for the Modulus Temperature Correction Program (MTCP)*; Texas A&M Transportation Institute: College Station, TX, USA, 2000.
38. Documenti Tecnici | Anas, S.p.A. Available online: <https://www.stradeanas.it/it/lazienda/attivita%20documenti-tecnici> (accessed on 10 July 2023).
39. Rada, G.; Witczak, M.W. Comprehensive Evaluation of Laboratory Resilient Moduli Results for Granular Material. *Transp. Res. Rec.* **1981**, *810*, 23–33.
40. Huang, Y.H. Stresses and Strains in Viscoelastic Multilayer Systems Subjected to Moving Loads. *Highw. Res. Rec.* **1973**, *457*, 60–71.
41. Zoccali, P.; Moretti, L.; Di Mascio, P.; Loprencipe, G.; D'Andrea, A.; Bonin, G.; Teltayev, B.; Caro, S. Analysis of Natural Stone Block Pavements in Urban Shared Areas. *Case Stud. Constr. Mater.* **2018**, *8*, 498–506. [[CrossRef](#)]
42. Clauß, M.; Wellner, F. Influence of the Load Position of Heavy Vehicles on the Service Life of Asphalt Pavements. *Int. J. Pavement Eng.* **2023**, *24*, 2149962. [[CrossRef](#)]
43. Chegenizadeh, A.; Keramatikerman, M.; Nikraz, H. Flexible Pavement Modelling Using Kenlayer. *Electron. J. Geotech. Eng.* **2016**, *21*, 2467–2479.
44. Kiran, S.; Madhu, K. Rutting and Fatigue Analysis of Flexible Pavement Using KENPAVE and IITPAVE: A Review. *J. Transp. Eng. Traffic Manag.* **2022**, *3*, 1–12.
45. Al Fatlawi, S.A.; Al-Jumaili, M.A. A Comparison of Viscoelastic Behaviour in Flexible Pavement Layers Responds to Different Contact Area. *AIP Conf. Proc.* **2024**, *3009*, 030105. [[CrossRef](#)]
46. Wang, F.; Machemehl, R.B. Mechanistic–Empirical Study of Effects of Truck Tire Pressure on Pavement: Measured Tire–Pavement Contact Stress Data. *Transp. Res. Rec.* **2006**, *1947*, 136–145. [[CrossRef](#)]
47. Taherkhani, H.; Moradloo, A.; Jalali Jirhandi, M. Investigation of the Effects of Tire Pressure on the Responses of Geosynthetic Reinforced Asphalt Pavement Using Finite Elements Methods. *Q. J. Transp. Eng.* **2016**, *8*, 323–342.
48. Boulos Filho, P.; Raymundo, H.; Machado, S.T.; Leite, A.R.C.A.P.; Sacomano, J.B. Configurations of Tire Pressure on the Pavement for Commercial Vehicles: Calculation of the 'N' Number and the Consequences on Pavement Performance. *Independ. J. Manag. Prod.* **2016**, *7*, 584–605. [[CrossRef](#)]
49. Collop, A.C.; Cebon, D. A Theoretical Analysis of Fatigue Cracking in Flexible Pavements. *Proc. Inst. Mech. Eng. Part C J. Mech. Eng. Sci.* **1995**, *209*, 345–361. [[CrossRef](#)]
50. Miner, M.A. Cumulative Damage in Fatigue. *J. Appl. Mech.* **1945**, *12*, A159–A164. [[CrossRef](#)]
51. Sybilski, D.; Bańkowski, W. Asphalt Pavement Design Using Results of Laboratory Fatigue Tests of Asphalt Mixtures. *Road Mater. Pavement Des.* **2002**, *3*, 183–194. [[CrossRef](#)]
52. Sudarsanan, N.; Kim, Y.R. A Critical Review of the Fatigue Life Prediction of Asphalt Mixtures and Pavements. *J. Traffic Transp. Eng. Engl. Ed.* **2022**, *9*, 808–835. [[CrossRef](#)]
53. Pellinen, T.K.; Christensen, D.W.; Rowe, G.M.; Sharrock, M. Fatigue-Transfer Functions: How Do They Compare? *Transp. Res. Rec.* **2004**, *1896*, 77–87. [[CrossRef](#)]
54. Sousa, J.B.; Ishai, I.; Svehinsky, G. Flexural Fatigue Tests and Predictions Models–Tools to Investigate SMA Mixes with New Innovative Binder Stabilizers. *Four-Point Bend.* **2012**, *1*, 171–188.
55. Shafabakhsh, G.H.; Sadeghnejad, M.; Sajed, Y. Case Study of Rutting Performance of HMA Modified with Waste Rubber Powder. *Case Stud. Constr. Mater.* **2014**, *1*, 69–76. [[CrossRef](#)]
56. Qiao, Y.; Flintsch, G.W.; Dawson, A.R.; Parry, T. Examining Effects of Climatic Factors on Flexible Pavement Performance and Service Life. *Transp. Res. Rec.* **2013**, *2349*, 100–107. [[CrossRef](#)]
57. Bruno, S.; Del Serrone, G.; Di Mascio, P.; Loprencipe, G.; Ricci, E.; Moretti, L. Technical Proposal for Monitoring Thermal and Mechanical Stresses of a Runway Pavement. *Sensors* **2021**, *21*, 6797. [[CrossRef](#)]
58. Fusco, R.; Moretti, L.; Fiore, N.; D'Andrea, A. Behavior Evaluation of Bituminous Mixtures Reinforced with Nano-Sized Additives: A Review. *Sustainability* **2020**, *12*, 8044. [[CrossRef](#)]

59. Bell, H.P.; Howard, I.L.; Freeman, R.B.; Brown, E.R. Evaluation of Remaining Fatigue Life Model for Hot-Mix Asphalt Airfield Pavements. *Int. J. Pavement Eng.* **2012**, *13*, 281–296. [[CrossRef](#)]
60. Ullidtz, P.; Harvey, J.; Tsai, B.-W.; Monismith, C. Calibration of CalME Models Using WesTrack Performance Data. In *Research Report: UCPRC-RR-2006-14*; University of California Pavement Research Center: Davis, CA, USA, 2006.

Disclaimer/Publisher’s Note: The statements, opinions and data contained in all publications are solely those of the individual author(s) and contributor(s) and not of MDPI and/or the editor(s). MDPI and/or the editor(s) disclaim responsibility for any injury to people or property resulting from any ideas, methods, instructions or products referred to in the content.